Composite Structures 251 (2020) 112601

Contents lists available at ScienceDirect

Composite Structures

journal homepage: www.elsevier.com/locate/compstruct

Spatio-temporally modulated composite metamaterials by using switchable mesostructural topology

Langquan Shui [a,*], Jiaojiao Guo [b], Enlai Gao [a,*], Ze Liu [a]

[a] Department of Engineering Mechanics, School of Civil Engineering, Wuhan University, Wuhan, Hubei 430072, China
[b] Department of Engineering Mechanics, School of Mechanics, Civil Engineering and Architecture, Northwestern Polytechnical University, Xi'an 710072, China

ARTICLE INFO

Keywords:
Spatio-temporally modulated composite metamaterial
Mesostructural topology
Acoustic switch
Virtual prototype

ABSTRACT

Spatio-temporally modulated composite metamaterials (STMCMs) possess tunable and nearly "full-banded" asymmetrical elastic wave properties, making them highly promising for uses in a wide range of applications, such as cloaking, acoustic information processing, ideal vibration isolation, ultrasonic technology. Despite much progress made in the structural design and fabrication of intelligent materials, the realization of STMCMs for practical fabrication is still an open issue because of a series of challenges existing in the rational design of the spatial and temporal ordered structures. In this work, we propose an implementation scheme for a laminated STMCM and computationally predict its performance. The elementary structure of the laminated STMCM is constructed by a functional component named as "acoustic switch" that endows the material with spatio-temporally modulated mesostructural topology and properties. This work not only provides a practical implementation scheme for experimental realization of the STMCMs, but also improves the understanding of STMCMs.

1. Introduction

Spatio-temporally modulated composite metamaterials (STMCMs), referring to the metamaterials with spatio-temporally modulated mesostructure, exhibit asymmetric wave properties, and hold great promises for uses in many exciting applications, such as cloaking, acoustic information processing, ideal vibration isolation and ultrasonic technology [1–14]. The elastic wave properties of STMCMs in the homogenization limit are predicted to exhibit strong Willis coupling (velocity-generated stresses or strain-generated momenta) [15–17], non-reciprocity, and time-reversal asymmetry [3,5]. It should be noted STMCMs have various names in the extensive studies, e.g. time–space modulated/active/dynamic/tunable/phase controlling/programmable/time dependent/time-varying (meta-) materials. Theoretically, as integrating active materials/mesostructures that are responsible to specific external stimuli, the hybrid structure will possess spatio-temporal modulable properties. However, the realization of STMCMs is still challenging in the rational design of the spatial and temporal ordered structures.

The early studies of the STMCMs appeared in last century [18–20], and significant achievements on mechanical STMCMs begins from the study of the linear elastic waves in transient materials by Weekes [21], Jensen [22], Rousseau and Maugin [23], Lurie [24] and their coworkers. Lurie and Weekes [25], and Sanguinet and Lurie [26] predicted a series of novel phenomena in a spatio-temporally modulated structure with periodic transient properties. Lurie [24] and Shui et al. [27] characterized the elastic wave propagation in a STMCM with one-dimensional (1D) moving properties interface (MPI). Considering 1D spatio-temporal periodicity, Lurie [24] first proposed a 1D metamaterial with asymmetrical wave property based on a homogenization method. Recently, for more general spatio-temporal periodicity, a lot of in-depth studies and extensions have been performed [4,28–32]. Remarkably, Shui et al. [28] and Nassar et al. [4] independently extend Lurie's homogenization theory to arbitrarily modulated periodic property profiles as well as to high dimensions. Meanwhile, Shui et al. [33] studied the property evolution in general spatio-temporally modulated materials and defined the property moving velocity ($\boldsymbol{V}$) as a function of spatio-temporal gradient of material property ($\boldsymbol{P}$), i.e.,

$$\boldsymbol{V} = -\frac{\partial \boldsymbol{P}}{\partial t} \cdot \frac{\nabla \boldsymbol{P}}{|\nabla \boldsymbol{P}|^2}. \tag{1}$$

* Corresponding authors.
E-mail addresses: l.q.shui@whu.edu.cn (L. Shui), enlaigao@whu.edu.cn (E. Gao).

https://doi.org/10.1016/j.compstruct.2020.112601
Received 26 February 2020; Revised 12 May 2020; Accepted 8 June 2020
Available online 10 June 2020

In addition, the property moving velocity can be also defined similar to Eq. (1) for STMCMs with discontinuous properties. Based on the definition of the property moving velocity of a MPI, Shui et al. [33,34] studied the elastic wave propagation law at three-dimensional (3D) MPI and proposed a scheme to solve the long-standing discontinuity and non-uniqueness problems when $|V|$ lies between the minimum and the maximum phase velocity of component materials [4,18,19,24].

Despite widespread interest and significant progress made in the study of STMCMs, practically speaking, the asymmetrical wave properties are still leaving unclear in the theory and numerical simulations [1,4,21,24,28,32,33] because of the challenging in the fabrication of an artificial structure with spatio-temporally as well as rapidly modulable properties. The basic governing equation for STMCMs is adopted from the classic wave equation [4,22,24,27,28,33] $\nabla \cdot \boldsymbol{\sigma} = \dot{\boldsymbol{p}} - \boldsymbol{f}$, where $\boldsymbol{\sigma}$, $\boldsymbol{p}$ and $\boldsymbol{f}$ are the stress, momentum and volume force, respectively. The underlying assumptions for the equation includes: (a) the external fields that modulate the properties do not couple with stress or momentum of the modulated system; (b) globally, the mechanical system obeys the momentum conservation during the property modulation process, and volume invariance at the mechanically equilibrium state. To satisfy these two requirements, seldom ready-found materials can be composited as a STMCM. For examples, the piezoelectric materials commonly exhibit coupling between mechanical and electrical fields, and the wave equation should be accompanied by a piezoelectric constitutive equation; and the shape memory materials have significant volume changes in the phase transition, and the wave equation should be modified by considering change of the initial configuration, i.e., mechanically equilibrium configuration. To this end, one should develop advanced and practical structure design to meet the abovementioned requirements. Besides, there are two additional requirements that should be noted: (c) to obtain the Willis coupling, the local density should be modulable. The significantly modulable density without global volume variance only can be realized by ingenious structural design. Thus, structural design is highly desirable; (d) to achieve strong Willis coupling, $|V|$ should be large enough and the modulating frequency of local property should be high enough, that is, the property modulating process should be extremely fast, which also causes considerable challenges in component material selection and subsequent structure design.

As indicated in the abovementioned four aspects, a rational structural design for the practical fabrication of STMCMs is highly desirable. Therefore, we proposes an implementation scheme for STMCMs accordingly, and break down the structural complexity of the proposed STMCMs into three levels, that is, the primary (component with an acoustic switch), secondary (hybrid unit constructed by one array of conductive acoustic switches and the other array of non-conductive acoustic switches) and tertiary (STMCM as the laminates of the hybrid units) levels. The work is arranged as following. An overview of STMCMs is given in Section 2. In Section 3, we introduce the primary structure consisting of an acoustic switch that can connect or disconnect the wave propagation path in real time and thus can be used to modulate topology of the mesostructure. In Section 4, the structure of the secondary level, especially the artificial interface between the arrays in the hybrid unit, is elaborated. In Section 5, the tertiary level of the laminated STMCM is constructed and its function is demonstrated. Finally, closing remarks is given in Section 6.

2. An overview of the STMCMs

The STMCMs have been briefly introduced in Section 1. This section focuses on providing an overview of the structure and wave property of STMCMs.

A traditional structural composite is constructed by spatially arranging of the unit cells, i.e., representative volume elements, and the actual properties $\boldsymbol{P}$ (e.g. the Young's modulus and density) can be expressed as periodic function with respect to spatial coordinates ($\boldsymbol{x} = (x, y, z) = (x_1, x_2, x_3)$) in the material framework, and the periods are the corresponding sizes of the unit cell ($\varepsilon_1 \times \varepsilon_2 \times \varepsilon_3$). Mathematically speaking, at the homogenization limit, $\varepsilon_1 \times \varepsilon_2 \times \varepsilon_3 \to 0$, and the properties are highly periodically oscillating with respect to $\boldsymbol{x}$. Under the assumption of linear elasticity, the mechanical properties can be described by the Adiabatic elastic tensor λ_{ijmn} and density ρ, and the governing equation for small deformation is,

$$\frac{\partial}{\partial x_j}\left(\lambda_{ijmn}(\boldsymbol{x})\frac{\partial u_m}{\partial x_n}\right) - \frac{\partial}{\partial t}\left(\rho(\boldsymbol{x})\frac{\partial u_i}{\partial t}\right) + f_i = 0, \tag{2}$$

where u_i and f_i are the displacement and the external volume force along the x_i–axis, respectively. At the homogenization limit, Eq. (2) is equivalent to the common linear elastic wave equation with constant coefficients,

$$\overline{\lambda}_{ijmn}\frac{\partial^2 u_m}{\partial x_j \partial x_n} - \overline{\rho}\frac{\partial^2 u_i}{\partial t^2} + f_i = 0, \tag{3}$$

where the homogenized Adiabatic elastic tensor $\overline{\lambda}_{ijmn}$ and density $\overline{\rho}$ can be uniquely determined by $\lambda_{ijmn}(\boldsymbol{x})$ and $\rho(\boldsymbol{x})$.

In abovementioned equations, the properties are considered as only the functions of $\boldsymbol{x}$, i.e., not related to time t. As proposing STMCMs, the time-varying properties should be considered, and the properties are also the function of t with period ε_4. Hence, Eq. (2) can be generalized as

$$\frac{\partial}{\partial x_j}\left(\lambda_{ijmn}(\boldsymbol{x}, t)\frac{\partial u_m}{\partial x_n}\right) - \frac{\partial}{\partial t}\left(\rho(\boldsymbol{x}, t)\frac{\partial u_i}{\partial t}\right) + f_i = 0, \tag{4}$$

which yields a generalized homogenized wave equation [28],

$$\overline{\lambda}_{ijmn}\frac{\partial^2 u_m}{\partial x_j \partial x_n} + \overline{\gamma}_{imn}\frac{\partial^2 u_m}{\partial t \partial x_n} - \overline{\rho}_i\frac{\partial^2 u_i}{\partial t^2} + f_i = 0, \tag{5}$$

where the homogenized properties $\overline{\lambda}_{ijmn}$, $\overline{\gamma}_{imn}$ and $\overline{\rho}_i$ can be uniquely determined by $\lambda_{ijmn}(\boldsymbol{x}, t)$ and $\rho(\boldsymbol{x}, t)$. Unlike Eq. (3), Eq. (5) predicts Willis coupling and asymmetrical wave properties [4,28] that cannot emerge in traditional materials. Therefore, these spatio-temporally ordered structural composites are named as STMCMs.

In the following, a 1D analysis is conducted to compare the behaviors of traditional structural composites and STMCMs. For example, considering longitudinal waves, λ_{ijmn} is replaced by the Young's modulus E. If the material properties are not related to time, Eq. (3) degenerates to

$$\overline{E}\frac{\partial^2 u_1}{\partial x^2} - \overline{\rho}\frac{\partial^2 u_1}{\partial t^2} + f_i = 0, \tag{6}$$

and the homogenized material properties are

$$\begin{cases} \overline{E} = \langle E^{-1}\rangle^{-1} \\ \overline{\rho} = \langle \rho \rangle \end{cases}, \tag{7}$$

only if E and ρ are well-defined everywhere and the operator $\langle\cdot\rangle$ represents taking its volume-averaged value, i.e., $\langle\cdot\rangle = \int_0^{\varepsilon_1}(\cdot)\mathrm{d}x/\varepsilon_1$. Let $f_i = 0$, Eq. (6) has the D'Alembert travelling wave solution,

$$u_x = f(x - \overline{c}t) + g(x + \overline{c}t), \tag{8}$$

where $f(x - \overline{c}t)$ and $g(x + \overline{c}t)$ are waves propagation along the $+x$ and $-x$ directions, respectively. These two waves have the same speed

$$\overline{c} = \sqrt{\overline{E}/\overline{\rho}}. \tag{9}$$

If the material properties are the function of time, Eq. (5) degenerates to the wave equation for 1D STMCMs

$$\overline{E}\frac{\partial^2 u_1}{\partial x^2} + \overline{\gamma}\frac{\partial^2 u_1}{\partial x \partial t} - \overline{\rho}\frac{\partial^2 u_1}{\partial t^2} + f_i = 0, \tag{10}$$

where the homogenized material properties can be given as (Taking $\boldsymbol{P} = \boldsymbol{P}(x - Vt)$, $\boldsymbol{P} = (E, \rho)$ as a specification) [28]

$$\begin{cases} \overline{E} = \langle E\xi \rangle^2 / \langle \xi \rangle - V^2 \langle \rho E \xi \rangle, \\ \overline{\gamma} = 2V[\langle \rho \xi \rangle \langle E\xi \rangle / \langle \xi \rangle - \langle \rho E \xi \rangle], \\ \overline{\rho} = \langle \rho E \xi \rangle - V^2 \langle \rho \xi \rangle^2 / \langle \xi \rangle, \end{cases} \tag{11}$$

where $\xi = 1/(E - \rho V^2)$, and V satisfies Eq. (1) in 1D form, i.e., $V = -\partial \boldsymbol{P}/\partial t \cdot (\partial \boldsymbol{P}/\partial x)/|\partial \boldsymbol{P}/\partial x|^2$. Note that the expressions in Eq. (11) were first formulated for arbitrary STMCMs by Lurie [24]. Let $f_i = 0$, Eq. (10) has a travelling wave solution,

$$u_1 = f(x - \overline{c}_1 t) + g(x - \overline{c}_2 t), \tag{12}$$

where

$$\begin{cases} \overline{c}_1 = \frac{-\overline{\gamma} + \sqrt{\overline{\gamma}^2 + 4\overline{\rho}\overline{E}}}{2\overline{\rho}} \\ \overline{c}_2 = \frac{-\overline{\gamma} - \sqrt{\overline{\gamma}^2 + 4\overline{\rho}\overline{E}}}{2\overline{\rho}} \end{cases} \tag{13}$$

If $\overline{c}_1$ is positive, $f(x - \overline{c}_1 t)$ is a wave propagating along the $+x$-direction with speed of $|\overline{c}_1|$, and $g(x - \overline{c}_2 t)$ is a wave propagating along the $-x$-direction with speed of $|\overline{c}_2|$. In general,

$$|\overline{c}_1| \neq |\overline{c}_2|. \tag{14}$$

This feature is quite different from traditional materials with identical wave velocity in opposite directions (i.e., $|\overline{c}_1| = |\overline{c}_2|$). For complex $\overline{c}_1$ with nonzero imaginary part, travelling wave cannot emerge in STMCMs, where the waves are localized near the wave source that is similar to the Saint-Vilan principle. In brief, Eqs. (12) to (14) demonstrate the asymmetric wave property in STMCMs (more details can be found in Appendix A).

In the derivation of Eq. (5), one retains the basic assumptions of Eq. (4), resulting in four difficult problems for experimental realization of the STMCMs. First, as shown in Eq. (4), the external fields that modulating the property should have no coupling with stress or momentum of the modulated system. Otherwise, additional equation should be introduced. Second, the mechanical system should obey the momentum conservation and volume invariance (at the mechanically equilibrium state) globally. Otherwise, strong nonlinearity would be introduced (refer to Appendix B), and the local initial state of the material would change with time [28]. Third, both the modulus and density should be time-varying. Otherwise, $\overline{\gamma}_{imn} = 0$, resulting in the disappearing of the asymmetric wave property. Forth, in the homogenization limit, $\varepsilon_4 \to 0$, which indicates that the modulating frequency of local property should be extremely high. To summarize, the structure/material requirements of STMCMs make it quite challenging for the design and fabrication, and traditional strategies of structural material design fail to meet these requirements. As a result, though STMCMs is highly promising for uses in many applications, such as cloaking, acoustic information processing, ideal vibration isolation, ultrasonic technology, a rational design for their realization is still challenging. To this end, we propose a novel scheme for realizing STMCMs by designing topology-modulable structures, which are presented as the following three levels.

3. Primary structure: acoustic switch

The wave behaviors are directly determined by the material properties in its propagation path. Thus, a simple idea is that the material properties can be tuned by modulating the wave propagation path. Such strategy can be achieved by designing structures with modulable topologies. Inspired by the switch of circuits that can change the current path, an "acoustic switch" is proposed. An acoustic switch is illustrated in Fig. 1. The open and close of switch is from contraction or expansion of a controllable active layer, which can be realized by a lot of smart materials, e.g. the piezoelectric ceramics. Note that width of the separation gap at the nonconductive state should be small to ensure rapid switch, and the compressive stress produced by the active layer at the conductive state should be large enough to ensure reliable connection. Meanwhile, the wavelength λ should be far larger than the size of the whole switch to avoid remarkable local effect arising from contraction or expansion of the active layer that would produce stress pulses.

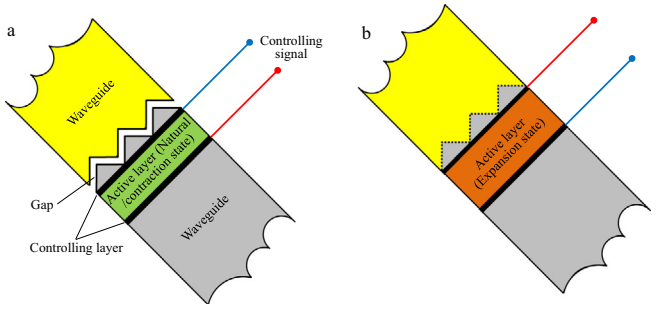

Fig. 1. Illustration of an acoustic switch based on contraction or expansion of a controllable active layer: (a) nonconductive state, (b) conductive state.

To demonstrate the feasibility of the acoustic switch, a virtual prototype is established by using COMSOL software. As shown in Fig. 2, a two-dimensional (2D) primary component consists of two square rings. The thickness of the primary component is 2 mm and its in-plane sizes are $a_x \times a_y = 1.5\sqrt{2} \times 3\sqrt{2}$ mm^2. The left ring is made by material A. The right one is made by material B with two synchronous lead zirconate titanate (PZT) based switches. Material A maintains continuous connectivity to ensure structural integrity. Illustration of the conductive and nonconductive states of the switches are shown in Fig. 2(b) and (c), respectively. Considering wave propagation along the x–axis , one can make an admittance analogy between the primary component and a circuit as shown in Fig. 2(d). In this analogy, there are the following analogy pairs: force ~ current I, velocity ~ voltage U, mass ~ capacitance C, modulus ~ reciprocal of the inductance $1/L$, damping ~ reciprocal of the electric resistance $1/R$, and force resistance and reactance ~ admittance Y. The current can flow through the green and blue components at the same time as the switch is

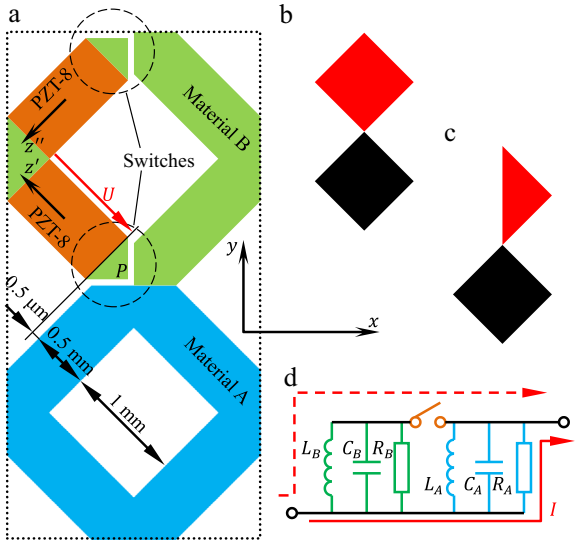

Fig. 2. A 2D primary structure: (a) component containing two synchronous acoustic switches, (b) and (c) the illustrations of the conductive and nonconductive states, and (d) circuit admittance analogy considering wave propagation along the x–axis in (a).

turned on while it can only flow through the blue components as the switch is turned off, that is,

$$U_{on} = I\left(Y_A^{-1} + Y_B^{-1}\right) \tag{15}$$

$$U_{off} = I/Y_A \tag{16}$$

Note that the property of the circuit can be described by the equivalent admittance that are $\left(Y_A^{-1} + Y_B^{-1}\right)^{-1}$ and Y_A at conductive and nonconductive states, respectively. Similarly, the acoustic switch can be expected to exhibit the function of the equivalent acoustic control.

A steady-state response analysis is performed to demonstrate the state switch function driven by external voltages, following by a harmonic response analysis to demonstrate the rapid response ability as required by STMCMs. The material properties are listed in Table 1. Considering the wavelength λ far larger than the size of primary component, only the internal force needs to be considered in the primary component, and the thermal expansion is ignored. Meanwhile, periodic boundaries are adopted at the dotted frame in Fig. 2(a), the internal boundaries in the switches are set as contact pairs with initial gap width of 0.5 μm, and other boundaries are free. The driven voltage, i.e., the electric potential difference along the z' or z'' –axis in the whole PZT, is U. In the steady-state response analysis, we can find that U of 0 and above 10 V can obtain nonconductive and reliable conductive states, respectively. The connection states at different driven voltages are shown in Fig. 3. The harmonic response of the state switch driven by harmonic voltages and characterized by total displacement of point P (Fig. 2(a)), is shown in Fig. 4. It can be expected that the switch exhibits best working state at $f_0 = 265$ kHz, which meets the requirement of high switch frequency for constructing STMCMs.

4. Secondary structure: Hybrids of an array of conductive acoustic switches and the other array of nonconductive acoustic switches

Starting from the proposed primary component, various spatio-temporally modulable structures can be constructed as inspired by the structure of the pixel point array [24,35]. To be specific, a primary component is similar to a pixel in a display, in which the properties (e.g. the modulus and density) are similar to the displayed color of the pixel. Similarly, the primary component array of acoustic switches can display material property distribution arbitrarily over time. MPI is the precondition for constructing the STMCMs due to the requirement of spatial and temporal order according to Eq. (1) [33]. The simple MPI is the static property interface (MPI with $V = 0$), which will be constructed as an example to demonstrate feasibility of this strategy.

4.1. Hybrid structure with a static property interface

Fig. 5(b) demonstrates two adjacent arrays of the primary components. The switches in the left part ($x < 100a_x$) of Fig. 5(b) are connected (voltage is 15 V, Fig. 5(a)), while switches in the right part ($x > 100a_x$) are disconnected (voltage is 0, Fig. 5(a)). The magnified view (the marks refer to Fig. 2(b, c)) in Fig. 5(b) demonstrates interface structures. To demonstrate its function, a longitudinal plane wave incidents from the left boundary (displacement $u_1 = 10^{-6}\exp\left[-4\times10^9\left(t-4.243\times10^{-5}\right)^2\right]$ (SI)) is simulated. The wave length is much larger than a_x. The wave induced displacement along the x–axis (u_1) on a path parallel to x–axis is shown in Fig. 5(c), where the path is shown in Fig. 5(b) by a yellow line in the magnified view. Note that the discontinuity of the curves in Fig. 5(c) is due to the material discontinuity along the path.

For 1D long wave, dynamic properties of the arrays (Fig. 5(b)) can be characterized by homogenized wave velocity $\bar{c}$ and wave impedance $\bar{z}$, where $\bar{c}$ can be directly recognized by wave propagation frames. The homogenized Young's modulus $\bar{E}$ can be calculated by a uniaxial tensile test along the x–axis (Fig. 5(d)). To be specific, an apparent pressure of 235.7 Pa is applied at the left boundary and the right boundary is fixed. Considering the relation $\bar{c} = \sqrt{\bar{E}/\bar{\rho}}$ (Eq. (9)), one can obtain the homogenized density

$$\bar{\rho} = \bar{E}/\bar{c}^2, \tag{17}$$

The homogenized material properties can be verified by the apparent reflected coefficient $R_{i,j}$ and transmitted coefficient $T_{i,j}$, which are well-known as

$$\begin{cases} R_{i,j} = \frac{z_i - z_j}{z_i + z_j}, \\ T_{i,j} = \frac{2z_i}{z_i + z_j}, \end{cases} \tag{18}$$

where the Latin subscript are free indexes, $z_i = \sqrt{\bar{E}_i\bar{\rho}_i}$. The indexes can be taken as "" that figuratively means array with nonconductive switches, or taken as "↔" that figuratively means array with conductive switches. The subscript "i,j" means that the incident wave is from material i, then transmits through the interface between material i and j, and finally propagates to material j.

According to Fig. 5(c), the homogenized wave velocities are extracted as $\bar{c} = 1124$ m/s and $\bar{c}_{\leftrightarrow} = 3182$ m/s. From Fig. 5(d), the homogenized Young's moduli are calculated as $\bar{E} = 3.978$ GPa and $\bar{E}_{\leftrightarrow} = 29.33$ GPa. According to Eq. (17), the homogenized densities are obtained as $\bar{\rho} = 3149$ kg/m^3 and $\bar{\rho}_{\leftrightarrow} = 2897$ kg/m^3. It is interesting that the array with conductive switches demonstrates a smaller homogenized density. Furthermore, the theoretical propagation coefficients can be calculated as (Eq. (18)) $R_{\leftrightarrow,} = 0.444$ and $T_{\leftrightarrow,} = 1.444$, which shows a difference of below 6% compared to the simulated results (Fig. 5(c), $R_{\leftrightarrow,} = 0.469$, $T_{\leftrightarrow,} = 1.464$) and indicates the validity and rationality of the homogenization method. A series of simulations are performed to investigate the effect of component properties on the homogenized properties, which demonstrate the excellent property-modulation ability of the primary structures Fig. 6. In addition, it is found that the mixed rules of the moduli and densities are similar to Eq. (11) ($V = 0$), i.e., the Young's modulus and homogenized density can be written as,

Table 1
Material properties in the primary component.

Materials	Density (kg/m^3)	Young's modulus (GPa) and Poisson's ratio/Elasticity matrix ** (GPa)	Coupling matrix ** (C/m^2)	Relative permittivity **	Loss factor
Material A *	2730	69 and 0.33	—	—	—
Material B	7850	200 and 0.30	—	—	—
PZT-8	7600	$\begin{bmatrix} 146.9 & 81.09 & 81.05 \\ 81.09 & 146.9 & 81.05 \\ 81.05 & 81.05 & 131.7 \\ & & 31.35 \\ & & 31.35 \\ & & 32.89 \end{bmatrix}$	$\begin{bmatrix} & 0 & \\ & & 10.34 \\ -3.875 & -3.875 & 13.91 \end{bmatrix}$	$\begin{bmatrix} 904.4 \\ 904.4 \\ 561.6 \end{bmatrix}$	0

* Material A is adopted from the Aluminum 3003-H18; material B is adopted from the High-strength alloy steel. ** The matrixes are given in local coordinates for cylindrically symmetric (∞mm) materials and the 3-direction is along the expansion direction (refer to z' and z'' –axis in Fig. 3).

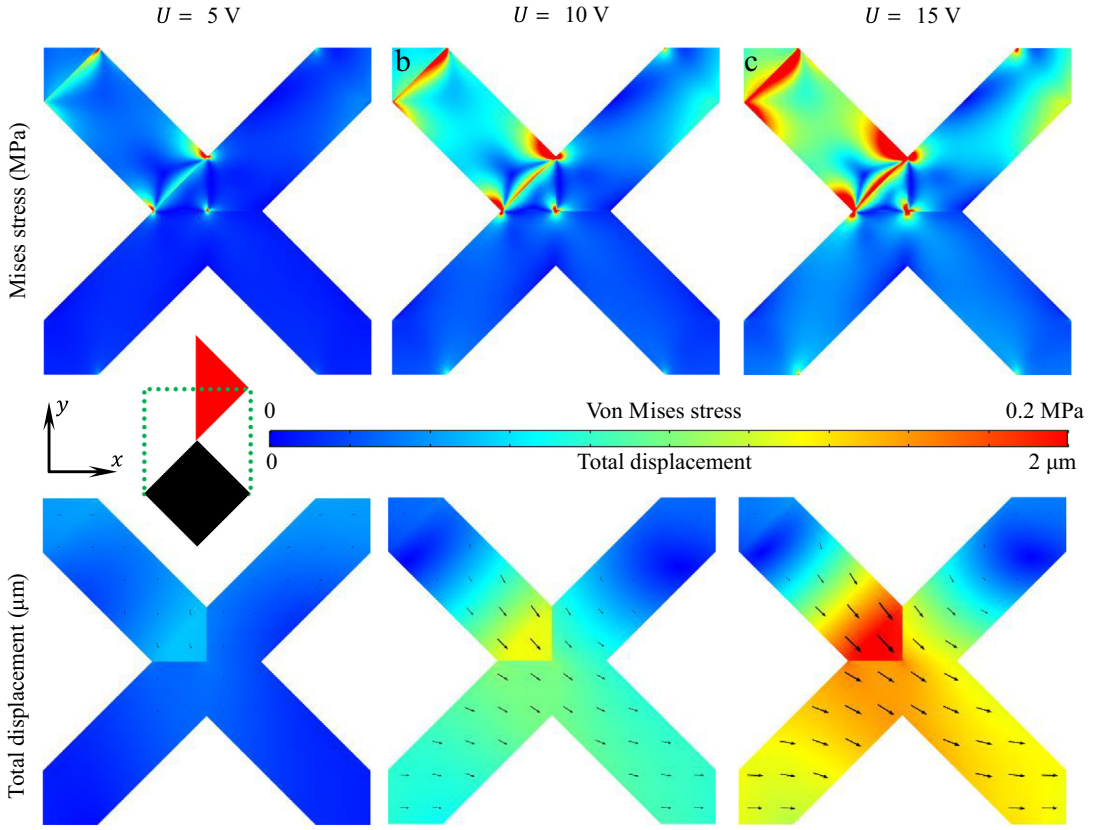

Fig. 3. Steady state response of the state switch of a primary component (only the part in the green dotted box is displayed): (a–c) Von Mises stress, and (d–f) total displacement. The actuation voltage in (a) and (d) is 5 V, (b) and (e) is 10 V, and (c) and (f) is 15 V. (For interpretation of the references to color in this figure legend, the reader is referred to the web version of this article.)

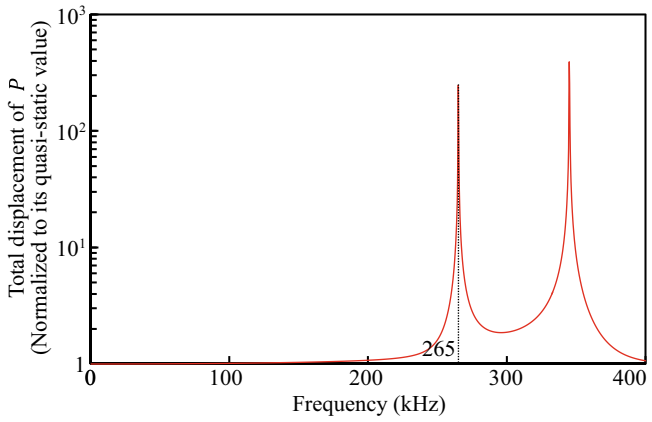

Fig. 4. Harmonic response of the primary component ($f_0 = 265$ kHz).

$$\begin{cases} \overline{E} = (a_1 + a_2/E_A + a_3/E_B)^{-1}, \\ \overline{\rho} = b_1 + b_2\rho_A + b_3\rho_B, \end{cases} \tag{19}$$

where a_i and b_i are constants ($i = 1, 2, 3$).

4.2. Hybrid structure with a moving property interface

Section 4.1 demonstrates that the primary components can form static interface and exhibit significant modulability of material property. Here we demonstrate the hybrid structure with a MPI. Different from the case in Fig. 5, the voltage is not static (Fig. 7(a)). The MPI moves forward for a distance $\Delta x = V\Delta t$ in a time interval Δt, and a switch changes between conductive and nonconductive state as the MPI passes through it (Fig. 7(b)). Considering the state switch time of a primary component $t_s > 0$, the MPI has a thickness

$$h = |V|t_s. \tag{20}$$

t_s should be half of the resonance period (Fig. 4), i.e., $t_s = 1.9$ μs for the structure in Fig. 2. To be specific, we set $V = -2000$ m/s, the MPI thickness h is 3.8 mm, which is about 1.8 times of the constant of primary component $a_x = 2.1$ mm. Considering that the wavelength λ is far larger than a_x, such thickness is small enough in the homogenization limit. Therefore, to form a sharp MPI, the switch delay time of an acoustic switch should be short enough (Eq. (20)), i.e., the resonance frequency should be high enough (Fig. 4). However, for a gradient MPI, i.e., with gradient distributed material properties in the interface, fast response of the switch is no longer necessary. Hence, forming a gradient interface is much easier than a sharp one in this way, which is contrary to the usual material interface.

To demonstrate the function of the MPI, a longitudinal plane wave incidents from the left boundary ($u_1 = 10^{-6}\exp\left[-4\times10^9(t-4.243\times10^{-5})^2\right]$ (SI)) is simulated. The results are shown in Fig. 7(c), in which we considered a typical case with $V = -2000$ m/s. According to the theory introduced in the previous work [27,33], as $\overline{c} < -V < \overline{c}_{\leftrightarrow}$, a normal incident wave on the MPI will produce three normal emitted waves (one reflected wave and two transmitted waves), which is supported by the numerical results with slight error (<8%, theoretical wavelength ratio should be $\left|\lambda : \lambda_R : \lambda_T : \lambda_T^{'}\right| = |(V-\overline{c}_{\leftrightarrow}) : (V+\overline{c}_{\leftrightarrow}) : (V-\overline{c}) : (V+\overline{c})| = 1 : 0.23 : 0.60 : 0.17$, and the propagation coefficients should be $R_{\leftrightarrow,} = (z_{\leftrightarrow} - z)/(z_{\leftrightarrow} + z)\cdot$

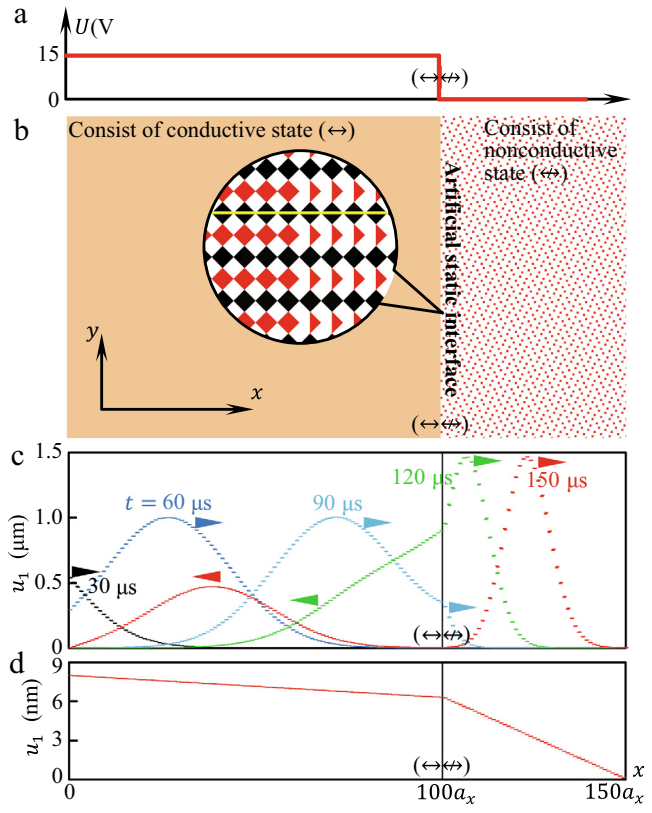

Fig. 5. Hybrid structure with an static property interface (MPI with $V = 0$): (a) local voltage electric potential difference in the PZT; (b) arrays with two states forming an artificial property interface; (c) simulated long elastic wave propagating along the yellow path in (b); (d) simulated uniaxial tension along the x–axis. Note that (a)–(d) share the same x–axis as shown in (d). (For interpretation of the references to color in this figure legend, the reader is referred to the web version of this article.)

$(c_{\leftrightarrow} + c)/(c_{\leftrightarrow} - c) \cdot (c_{\leftrightarrow} - |V|)/(c_{\leftrightarrow} + |V|) = 0.21$, $T_{\leftrightarrow,} = 1 + R_{\leftrightarrow,} - T'_{\leftrightarrow,} = 1.63$, and $T'_{\leftrightarrow,} = (z_{\leftrightarrow} - z)/z \cdot c_{\leftrightarrow}/(c_{\leftrightarrow} - c) \cdot (c - |V|)/(c_{\leftrightarrow} + |V|) = -0.42$, here the symbols with apostrophe corresponds to the backward conjugate transmitted wave. The derivation of these equations can be found in Refs [33,34]). To summarize, a hybrid structure with a MPI is successfully constructed by primary components, which is expected to be used in STMCMs.

5. Tertiary structure: Laminated STMCMs

Layer-by-layer assembling of secondary structures can form a 2D laminated STMCM [28] (Fig. 8(a)). In this STMCM, the unit cell constants can be represented by $\boldsymbol{\varepsilon} = (\varepsilon_x, \varepsilon_y; \varepsilon_t)$, where ε_x and ε_y is the spatial period, and ε_t is the temporal period of the acoustic switch (Fig. 8 (b)). For the laminated STMCM,

$$\begin{cases} a_x \ll \varepsilon_x \ll \lambda, \\ \varepsilon_y = a_y, \\ \varepsilon_t = \varepsilon_x/|V|. \end{cases} \tag{21}$$

The first line in Eq. (21) indicates that the STMCM is a three-level composite. Fig. 8(c) demonstrates the voltage–time curve of one acoustic switch in the STMCM, and the right adjacent one has the similar curve but a phase shift of

$$\Delta\varphi = -\frac{2\pi a_x}{\varepsilon_x}\frac{V}{|V|}. \tag{22}$$

According to Eq. (21), in the design of an acoustic switch, the working frequency f_0 (Fig. 4) should meet

$$f_0 = \frac{2\pi}{\varepsilon_t} = 2\pi\frac{|V|}{\varepsilon_x}. \tag{23}$$

To demonstrate the function of the laminated STMCM, two longitudinal plane waves incident from the left and right boundaries ($u_1 = 10^{-6}\exp\left[-4\times10^7\left(t - 6.364\times10^{-4}\right)^2\right]$ (SI)) are simulated. The results are shown in Fig. 8(d), in which $V = 1000$ m/s, $\varepsilon_x = 10a_x$, i.e., $\varepsilon_t = 21$ μs (Eq. (21)) and the switch frequency should be $f_0 \approx 299$ kHz (Eq. (23)). According to the theory in the previous work [24,28] and that introduced in Section 2, the normal incident waves from opposite directions have different group velocities, i.e., homogenized wave velocity (Referring to Eq. (13), the theoretical group velocities should be 1230 m/s along the $+x$-direction and 1310 m/s along the $-x$-direction). These results are supported by the numerical simulations with an error of below 20%. It should be noted that this error arises from the numerical challenging in the simulation of a time dependent/energy opening oscillating system [28,36]. In summary, a laminated STMCM is successfully constructed from the hybrids of arrays of acoustic switches, which provides an implementation scheme for STMCMs.

6. Closing remarks

In summary, this work proposes an implementation scheme for the realization of STMCMs and demonstrates its fantastic performances.

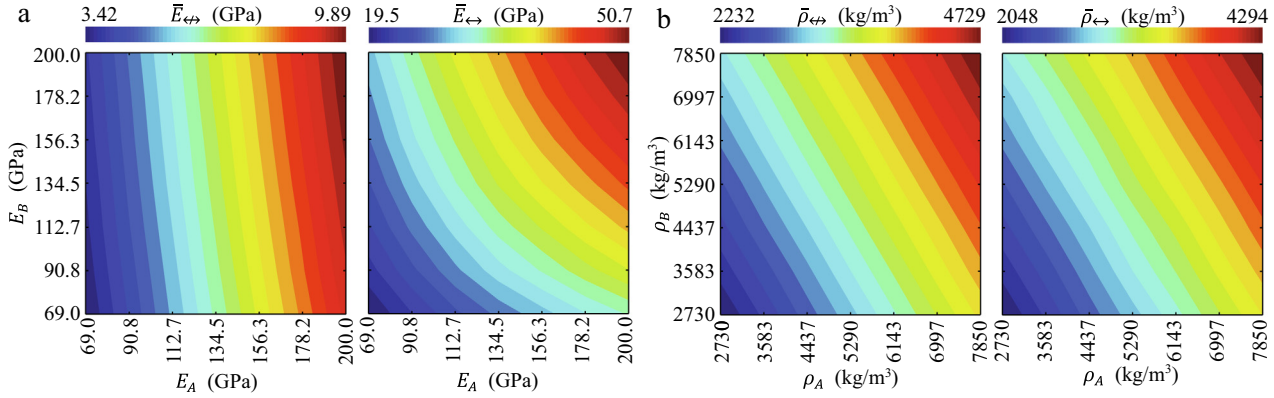

Fig. 6. Component properties determine the homogenized properties of the secondary structure. The calculated homogenized properties are $\bar{E} = (0.0059 + 17.16/E_A + 1.339/E_B)^{-1}$ (Unit: GPa; R-square: 0.9969), $\bar{E}_{\leftrightarrow} = (0.0044 + 1.784/E_A + 1.295/E_B)^{-1}$ (Unit: GPa; R-square: 0.9913), $\bar{\rho} = 900.7 + 0.3084\rho_A + 0.18\rho_B$ (Unit: kg/m^3; R-square: 1), and $\bar{\rho}_{\leftrightarrow} = 844.1 + 0.274\rho_A + 0.1658\rho_B$ (Unit: kg/m^3; R-square: 0.9999).

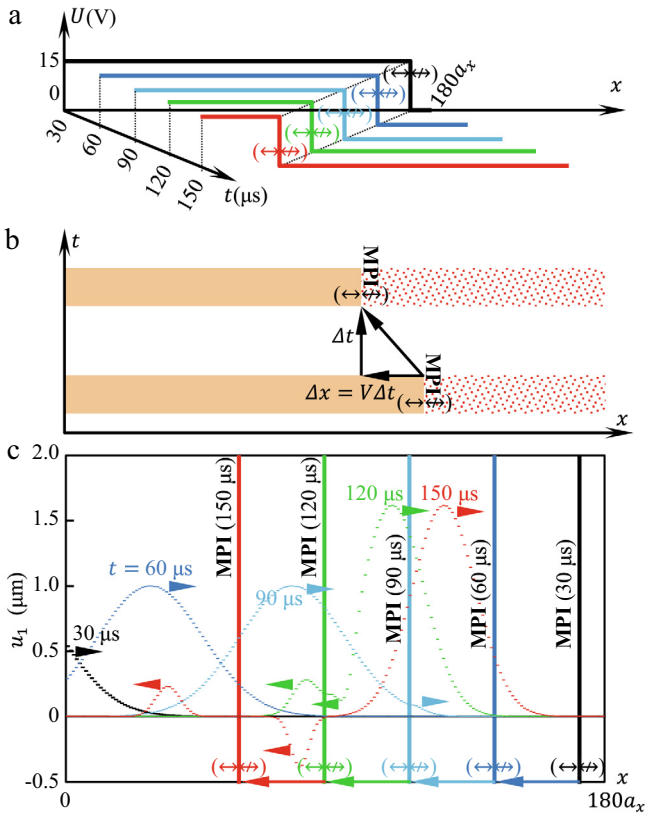

Fig. 7. Hybrid structure with a MPI: (a) local voltage electric potential difference in the PZT; (b) acoustic switch induced property interface motion; (c) simulated long elastic wave propagating along the yellow path in Fig. 5(b) through the MPI. Colors of the lines in (a) and (c) correspond to the marked time in (c). (For interpretation of the references to color in this figure legend, the reader is referred to the web version of this article.)

The spatio-temporally modulated properties of the proposed STMCMs are realized by acoustic switches that could rapidly disconnect or connect the propagation path of the elastic waves upon external signals. The demonstration are supported by both theory and numerical simulations, demonstrating the feasibility of the implementation scheme for STMCMs. This work sheds light on the experimental realization of STMCMs.

CRediT authorship contribution statement

Langquan Shui: Conceptualization, Methodology, Software, Writing - original draft, Visualization, Supervision, Funding acquisition. **Jiaojiao Guo:** Validation, Formal analysis, Data curation, Visualization. **Enlai Gao:** Methodology, Resources, Writing - review & editing, Supervision, Funding acquisition. **Ze Liu:** Writing - review & editing, Funding acquisition.

Declaration of Competing Interest

The authors declare that they have no known competing financial interests or personal relationships that could have appeared to influence the work reported in this paper.

Acknowledgements

This work is supported by the National Natural Science Foundation of China (11632009, 11872284, 11902225, 11902226) and Fundamental Research Funds for the Central Universities (413000111, 413000114).

Appendix A. Comparison of the wave properties between traditional structural composites and STMCMs

One can describe the wave properties by the group velocity surfaces. As examples, the group velocities of two laminated composites that are governed by Eqs. (3), (5), and (10) are illustrated in Fig. A1, which demonstrates the difference of wave properties between traditional structural composites and STMCMs. The material properties and formula for group velocity calculation in Fig. A1 can be referred below.

For simplification, Eqs. (3) and (5) are rewritten in an unified form as following [28]

$$\frac{\partial}{\partial x_\alpha}\left(\bar{\lambda}_{i\alpha m\beta}\frac{\partial u_m}{\partial x_\beta}\right) = -f_i, \tag{A.1}$$

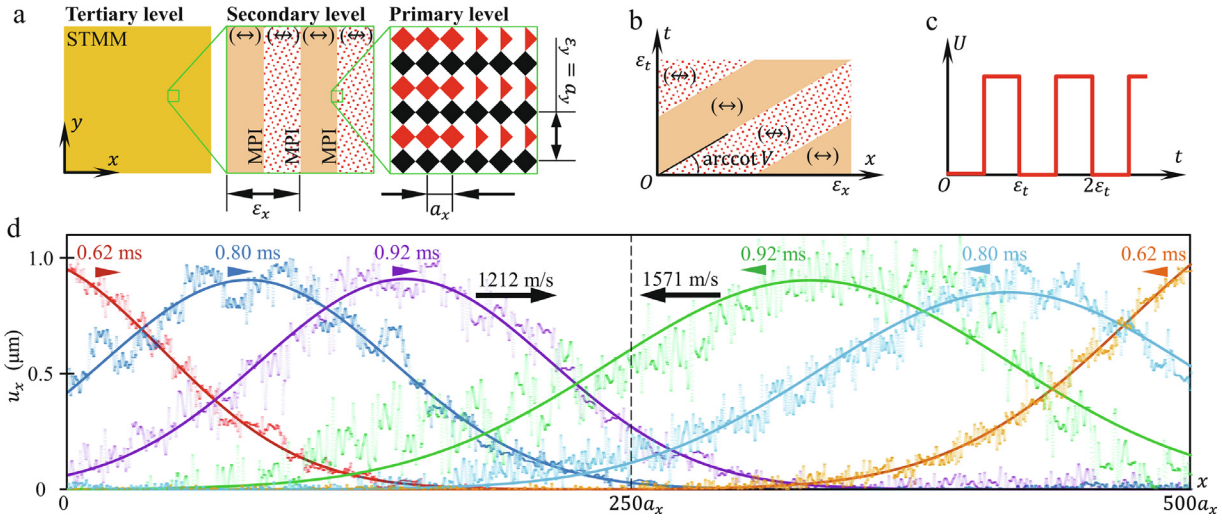

Fig. 8. A laminated STMCM: (a) three level structures of a laminated STMCM; (b) a spatio-temporal unit cell of the STMCM; (c) the voltage electric potential difference in an acoustic switch; (d) simulated long elastic waves ($a_x \ll \varepsilon_x \ll \lambda$) propagating through the STMCM (the original data from numerical simulation is provided, and the solid lines represent the fitting curves using Gauss function).

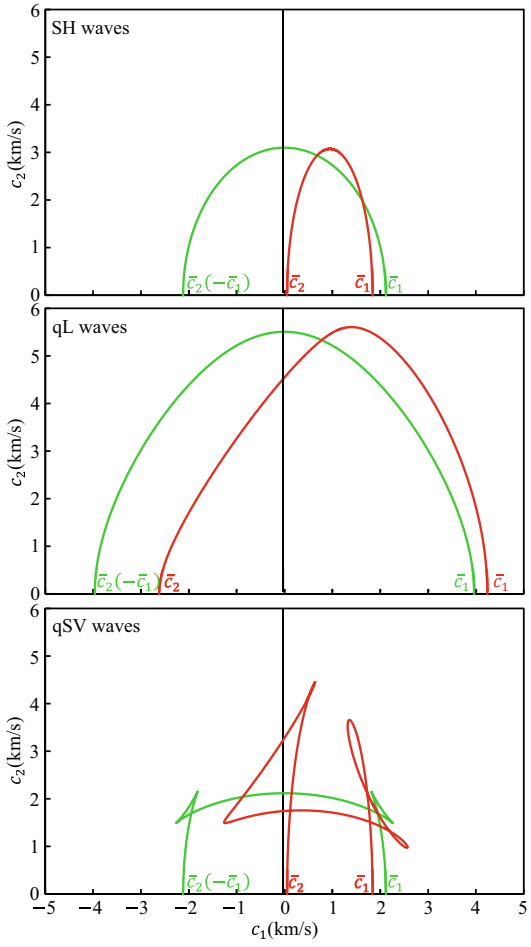

Fig. A1. Group velocities of a traditional laminated composite (green lines) and laminated STMCM (red lines). c_i refer to Eq. (A.2), and $\bar{c}_1$ and $\bar{c}_2$ refer to Eq. (13). The curves mean the positions that the disturbance at the origin can propagate to in an unit time. (For interpretation of the references to color in this figure legend, the reader is referred to the web version of this article.)

where $\bar{\lambda}_{i\alpha m\beta} = \bar{\lambda}\delta_{i\alpha}\delta_{m\beta} + \bar{\mu}\left(\delta_{im}\delta_{\alpha\beta} + \delta_{i\beta}\delta_{\alpha m}\right) - (\bar{\mu}+\bar{\rho})\delta_{\alpha 4}\delta_{\beta 4}\delta_{im}$, $\bar{\lambda}$ and $\bar{\mu}$ are the homogenized Lame constant; the Latin index takes 1 to 3, and the Greek index takes 1 to 4 and "4" corresponds to time t. When $\alpha,\beta \neq 4$, $\bar{\lambda}_{i\alpha m\beta}$ degenerates to the Adiabatic elastic tensor; when $\alpha,\beta = 4$ and $i = m$, $-\bar{\lambda}_{i\alpha m\beta}$ degenerates to the homogenized density $\bar{\rho}$; otherwise, $\bar{\lambda}_{i\alpha m\beta} = 0$. Obviously, $\bar{\gamma}_{imn} = \bar{\lambda}_{i4mn} + \bar{\lambda}_{inm4}$, $\bar{\rho}_i = -\bar{\lambda}_{i4\,i\,4}$. By using the symbol $\bar{\lambda}_{i\alpha m\beta}$, the material properties (adopted from Shui et al. [28]) is listed in Tables A1 and A2 for a traditional laminated composite and laminated STMCM, respectively.

Considering a wave with a circular frequency of ω: $u_i = U_i \exp\left[\sqrt{-1}(k_j x_j - \omega t)\right]$, where the amplitude U_i determines the polarization direction, and k_j is the wave vector. For Eq. (5), the dispersion relation can be derived as $\left|\bar{\lambda}_{ijmn}k_j k_n - \bar{\gamma}_{imn}k_n\omega - \bar{\rho}_i\delta_{im}\omega^2\right| = 0$. Then one can derive the group velocity as

$$c_i = \frac{\partial\omega}{\partial k_i} = \frac{\left(2\bar{\lambda}_{kimn}k_n - \bar{\gamma}_{kmi}\omega\right)U_k U_m}{\bar{\gamma}_{qrs}k_s U_r U_q + 2\omega\bar{\rho}_s U_s^2}. \tag{A.2}$$

Note that ω in Eq. (A.2) is a function of the direction of a wave vector, and it can be solved by the dispersion relation. In particular, by letting $\bar{\gamma}_{kmi} = 0$ and $\bar{\rho}_i = \bar{\rho}$, Eq. (A.2) is also valid for Eq. (3).

Finally, by using Eqs. (A.1) and (A.2) and the parameters given in Tables A1 and A2, the group velocities can be calculated (Fig. A1).

Appendix B. Notes for the momentum conservation in STMCMs

The 1D situation with a uniform time-varying density (here the modulus has no effect on momentum and is set as passive) is considered (any time-varying property can be transformed into a combination of a serials of the elementary uniform time-varying property). Considering a material with property

$$\boldsymbol{P} = \begin{cases} \boldsymbol{P}_1, t < t_0, \\ \boldsymbol{P}_2, t \geq t_0, \end{cases} \tag{B.1}$$

where $\boldsymbol{P}_i = (E, \rho_i), i = 1, 2$.

Suppose that there is a travelling wave $u_1(x - c_1 t)$ ($c_i = \sqrt{E/\rho_i}$) in the material before the time t_0. At the time oft_0, the density of the material increases by $\Delta\rho = \rho_2 - \rho_1$, and the momentum increases by Δp. Based on the momentum theorem $(\rho_1 + \Delta\rho)v_{20} = \rho_1\partial u_1/\partial t + \Delta p$, where v_{20} is the particle velocity after the density change, $v_{20} = \rho_1/\rho_2 \cdot \partial u_1/\partial t + \Delta p/\rho_2$. Furthermore, according to the wave equation $c_2^2\partial^2 u_2/\partial x^2 = \partial^2 u_2/\partial t^2, (x,t) \in \mathbf{R} \times [t_0, +\infty)$, we have a D'Alembert travelling wave solution as

$$u_2 = \frac{z_2 + z_1}{2z_2}u_1(x - c_2 t) + \frac{z_2 - z_1}{2z_2}u_1(x + c_2 t) + \frac{1}{2z_2} \times \int_{x-c_2 t}^{x+c_2 t} \Delta p \mathrm{d}x, t \geq t_0, \tag{B.2}$$

where $z_i = \sqrt{E\rho_i}$.

Eq. (B.2) indicates that the waveforms change as the momentum changes, i.e., the linear property of the wave equation is broken. It can be expected that different mechanisms of density change can induces different forms of Δp, and Δp may relate to the current deformation and velocity. In most cases, the existence of Δp would make the issue difficult to be addressed. For the sake of simplicity, we consider

Table A1
Material properties of a laminated traditional composite for Fig. A1 (Normal direction of the layers is along the $x$axis. Units: GPa, kg/m^3).

$i\alpha$	$m\beta$											
	11	22	33	23	32	13	31	12	21	14	24	34
11	126	53.9	53.9									
22	53.9	243.0	89.0									
33	53.9	89.0	243									
23				76.9	76.9							
32				76.9	76.9							
13						35.9	35.9					
31						35.9	35.9					
12								35.9	35.9			
21								35.9	35.9			
14										–8000		
24											–8000	
34												–8000

Table A2
Material properties of a laminated STCMM for Fig. A1 (Normal direction of the layers is along the x–axis. Units: GPa, kg/s/mm^2, kg/m^3).

$i\alpha$	$m\beta$											
	11	22	33	23	32	13	31	12	21	14	24	34
11	91.5	50.1	50.1							–2.17		
22	50.1	241	87.4							–93.0		
33	50.1	87.4	241							–93.0		
23				76.9	76.9							
32				76.9	76.9							
13						25.4	25.4					–2.57
31						25.4	0.763					–2.57
12								25.4	25.4		–2.57	
21								25.4	0.763		–2.57	
14	–2.17	–93.0	–93.0							–8030		
24								–2.57	–2.57		–8130	
34						–2.57	–2.57					–8130

$$\Delta p \equiv 0. \tag{B.3}$$

Appendix C. Supplementary data

Supplementary data to this article can be found online at https://doi.org/10.1016/j.compstruct.2020.112601.

References

[1] Huang JH, Zhou XM. A time-varying mass metamaterial for non-reciprocal wave propagation. Int J Solids Struct 2019;164:25–36.
[2] Monticone F, Valagiannopoulos C, Savoia S, Fleury R, Alu A. PT-Symmetric Metamaterial Systems for Aberration-Free Imaging and Wave Manipulation. 9th International Congress on Advanced Electromagnetic Materials in Microwaves and Optics (Metamaterials 2015). 2015:223-5.
[3] Zhu XF, Ramezani H, Shi CZ, Zhu J, Zhang X. PT-Symmetric Acoustics. Physical Review X. 2014;4:031042.
[4] Nassar H, Xu XC, Norris AN, Huang GL. Modulated phononic crystals: non-reciprocal wave propagation and Willis materials. J Mech Phys Solids 2017;101:10–29.
[5] Fleury R, Sounas D, Alu A. An invisible acoustic sensor based on parity-time symmetry. Nat Commun 2015;6:5905.
[6] Fleury R, Sounas DL, Khanikaev A, Alu A. Breaking Temporal Symmetries in Acoustic Metamaterials. 9th International Congress on Advanced Electromagnetic Materials in Microwaves and Optics (Metamaterials 2015). 2015:358-60.
[7] Bao B, Wang Q. Elastic wave manipulation in piezoelectric beam meta-structure using electronic negative capacitance dual-adjacent/staggered connections. Compos Struct 2019;210:567–80.
[8] Huang LX, Duan YP, Yang X, Gao SH, Zeng YS, Ma GJ, et al. Ultra-flexible composite metamaterials with enhanced and tunable microwave absorption performance. Compos Struct UNSP 2019;229:111469.
[9] Li X, Zhu Y, Liu X, Xu BB, Ni Q. A broadband and tunable microwave absorption technology enabled by VGCFs/PDMSEP shape memory composites. Compos Struct 2020;238:111954.
[10] Lim TC. A composite metamaterial with sign switchable elastic and hygrothermal properties induced by stress direction and environmental change reversals. Compos Struct 2019;220:185–93.
[11] Salighe S, Mohammadi H. Semi-active nonlinear vibration control of a functionally graded material rotating beam with uncertainties, using a frequency estimator. Compos Struct 2019;210:367–80.
[12] Zhang K, Su YC, Zhao PC, Deng ZC. Tunable wave propagation in octa-chiral lattices with local resonators. Compos Struct 2019;220:114–26.
[13] Yi KJ, Matten G, Ouisse M, Sadoulet-Reboul E, Collet M, Chevallier G. Programmable metamaterials with digital synthetic impedance circuits for vibration control. Smart Mater Struct 2020;29:035005.
[14] Yi KJ, Ouisse M, Sadoulet-Reboul E, Matten G. Active metamaterials with broadband controllable stiffness for tunable band gaps and non-reciprocal wave propagation. Smart Mater Struct 2019;28:065025.
[15] Willis JR. A polarization approach to the scattering of elastic-waves. 2. Multiple-scattering from inclusions. J Mech Phys Solids 1980;28:307–27.
[16] Willis JR. A polarization approach to the scattering of elastic-waves. 1. Scattering by a single inclusion. J Mech Phys Solids 1980;28:287–305.
[17] Willis JR. The construction of effective relations for waves in a composite. CR Mec 2012;340:181–92.
[18] Cassedy ES, Oliner AA. Dispersion relations in time-space periodic media: part I-stable interactions. Proc IEEE 1963;51:1342–59.
[19] Cassedy ES. Dispersion relations in time-space periodic media: part II-Unsta- ble interactions. Proc IEEE 1967;55:1154–68.
[20] Slater JC. Interaction of waves in crystals. Rev Mod Phys 1958;30:197–222.
[21] Weekes SL. A stable scheme for the numerical computation of long wave propagation in temporal laminates. J Comput Phys 2002;176:345–62.
[22] Jensen JS. Space-time topology optimization for one-dimensional wave propagation. Comput Methods Appl Mech Eng 2009;198:705–15.
[23] Rousseau M, Maugin GA, Berezovski M. Elements of study on dynamic materials. Arch Appl Mech 2011;81:925–42.
[24] Lurie KA. An Introduction to the Mathematical Theory of Dynamic Materials. Springer, New York, NY. 2007.
[25] Lurie KA, Weekes SL. Wave propagation and energy exchange in a spatio-temporal material composite with rectangular microstructure. J Mathemat Anal Appl 2006;314:286–310.
[26] Sanguinet WC, Lurie KA. Propagation of dilatation and shear waves through a dynamic checkerboard material geometry in 1D space + time. Zamm-Zeitschrift Angew Mathematik Mechanik 2013;93:937–43.
[27] Shui LQ, Yue ZF, Liu YS, Liu QC, Guo JJ. One-dimensional linear elastic waves at moving property interface. Wave Motion 2014;51:1179–92.
[28] Shui LQ, Yue ZF, Liu YS, Liu QC, Guo JJ, He XD. Novel composites with asymmetrical elastic wave properties. Compos Sci Technol 2015;113:19–30.
[29] Milton GW, Mattei O. Field patterns: a new mathematical object. Proceedings of the Royal Society A-Mathematical Physical and Engineering Sciences. 2017;473:20160819.
[30] Swinteck N, Matsuo S, Runge K, Vasseur JO, Lucas P, Deymier PA. Bulk elastic waves with unidirectional backscattering-immune topological states in a time-dependent superlattice. J Appl Phys 2015;118:063103.
[31] Trainiti G, Ruzzene M. Non-reciprocal elastic wave propagation in spatiotemporal periodic structures. New J Phys 2016;18:083047.
[32] Vila J, Pal RK, Ruzzene M, Trainiti G. A Bloch-based procedure for dispersion analysis of lattices with periodic time-varying properties. J Sound Vib 2017;406:363–77.
[33] Shui LQ, Liu YL, Chen X. Three dimensional wave propagation in time-varying materials: a mathematical model based on the weak solutions of continuity in the moving property interface. Appl Math Model 2017;48:134–52.
[34] Shui LQ, Liu YL, Chen X. Snell's law of elastic waves propagation on moving property interface of time-varying materials. Int J Solids Struct 2018;143:18–28.
[35] Pan F, Li YL, Li ZY, Yang JL, Liu B, Chen YL. 3D pixel mechanical metamaterials. Adv Mater 2019;31:1900548.
[36] Dong QL, Cao LQ. Multiscale asymptotic expansions and numerical algorithms for the wave equations of second order with rapidly oscillating coefficients. Appl Numer Math 2009;59:3008–32.